Heliyon 6 (2020) e03237

Contents lists available at ScienceDirect

Heliyon

journal homepage: www.cell.com/heliyon

Review article

Photocatalytic activity and doping effects of $BiFeO_3$ nanoparticles in model organic dyes

A. Haruna *, I. Abdulkadir, S.O. Idris

Department of Chemistry, Ahmadu Bello University, Zaria, Nigeria

ARTICLE INFO

Keywords:
Materials science
Nanotechnology
Inorganic chemistry
Doping
$BiFeO_3$
Pollutants
Organic dyes
Photocatalyst
Nanoparticles

ABSTRACT

The studies of advanced materials in environmental remediation and degradation of pollutants is rapidly advancing because of their wide varieties of applications. $BiFeO_3$ (BFO), a perovskite nanomaterial with a rhombohedral *R3c* space group, is currently receiving tremendous attention in photodegradation of dyes. The photocatalytic activity of BFO nanoparticle is a promising field of research in photocatalysis. BFO nanomaterial is a photocatalyst enhanced by doping because of its reduce bandgap energy (2.0–2.77 eV), multiferroic property, strong photoabsorption and crystal structure. The material has proven to be very useful for the degradation of dyes under visible light irradiation among other photocatalysts. Its exceptional nontoxicity, suitability, low cost and long term excellent stability makes it an efficient photocatalyst for the degradation of effluents from textile and pharmaceutical industries which ended-up in the environment and now a major concern of the modern world. This mini-review attempts to provide some detailed synthetic routes of BFO and BFO related nanomaterials and the notable achievements so far on the effect of doping the material. It also discusses the effect of crystallite size of the material and other photophysical properties and how they influence the photocatalytic process of model organic dye pollutants, to date.

1. Introduction

Recently, the photocatalytic and multiferroic properties, magnetic ordering and doping effects of $BiFeO_3$ (BFO) is an area of growing interest in modern scientific research. BFO nanoparticle is a semiconductor material capable of displaying potential applications in piezoelectric devices, sensors, photosensitizers, and spintronics (Zhao et al., 2008; Zeches et al., 2009; Yu et al., 2009; Jiang et al., 2011). The material has a narrow bandgap of about 2.2 eV compared to the widely used TiO_2 with energy bandgap of 3.2 eV (Niu et al., 2015a). A narrow bandgap provides the possibility of using a large portion of visible light from the total solar energy. This is important to increase the solar energy utilization efficiency because the current TiO_2 photocatalysts can generally response only in the UV range due to its large energy bandgap (Zhang et al., 2012; Liu et al., 2012). Fast recombination of electrons and holes during photocatalysis is another problem which also lowers the efficiency of photocatalyst (Rajeshwar et al., 2008). In addition, BFO hold a great promise because of its numerous technological application in photodegradation of organic dyes, wastewater treatments, air purification processes, photovoltaic and in water splitting for hydrogen production to generate clean energy (Maeda and Domen, 2007; He et al., 2013; Hu et al., 2017; Moniruddin et al., 2018). BFO material is an inorganic perovskite under the ferrites that is a visible light-driven photocatalyst.

Perovskite nanomaterials are class of materials with a general formula of ABX_3 wherein its crystal structure A and B represents metal ions of the periodic table and X indicates an anionic group (Cl^-, Br^-, I^-, O^{2-}) (Yang et al., 2006; Cheng and Lin, 2010; Kanhere and Chen, 2014). The photocatalytic activity of these perovskite materials can be improved by doping considering the wide scope of design to alter both A and B sites. Studies have shown that doping of the material at either of the sites gives it extra photocatalytic advantage to reduce the bandgap and other photophysical properties of these functional oxides (Shi and Guo, 2013). Figure 1a shows the perovskite structure consisting of the cation sites in the crystal lattice and how B and X form an octahedral BX_6 structure, where at the center of the octahedral structure, X lies in the corners around B. The A- site (Bi in BFO) is located on the corners of the unit cell and the B- site (Fe in BFO) at the center of the unit cell (Lam et al., 2017). Figure 1b shows the formation of a 3-D system of an octahedral structure in an extended form linking each other at all-corners of the structure. For effective charge neutrality, however, the metal A, in the crystal structure

* Corresponding author.
E-mail address: abdurrashid.haruna@yahoo.com (A. Haruna).

https://doi.org/10.1016/j.heliyon.2020.e03237
Received 22 November 2019; Received in revised form 9 January 2020; Accepted 13 January 2020

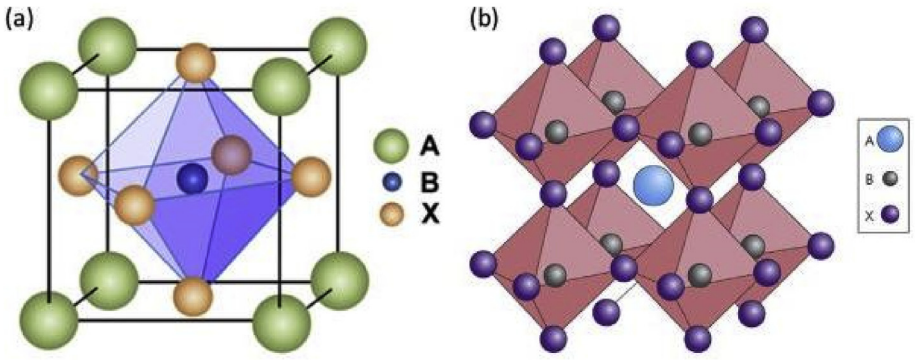

Figure 1. (a) A perovskite unit cell (ABX_3), and (b) extended network structure of perovskites linked via the corner-shared octahedral. Reprinted from Refs (Park, 2016; Green et al., 2014).

located in a vacancy within the BX_6 structure maintain the overall charge of the structure and the metal B is filling the octahedral sites (Tanaka and Misano, 2001). BFO nanoparticle exhibits a distorted rhombohedral perovskite structure with *R3c* space group at room temperature.

The studies of BFO and BFO related particles and their visible light (λ = 200–800 nm) response is particularly interesting because of their excellent nontoxicity, cost effectiveness, special crystallite structure, electrical conductivity, long-term stability, magnetism and electro-optical properties which makes them efficient photocatalyst (Liu et al., 2007; Chen and Mao, 2007; Carp et al., 2004; Asahi et al., 2001). The effect of doping BFO material with noble elements has opened-up new opportunities to develop novel materials that can improve on photocatalytic activity (Gao et al., 2007; Zhang et al., 2015a,b; Wang et al., 2016). Doping is one most important way to efficiently enhance the photocatalytic performance of BFO and other related materials especially with the rare-earth (RE) elements. The RE elements can facilitate the abruption of photogenerated electron-hole ($e- h^+$) pairs because of their special 4f electron configurations (Wu et al., 2012; Pei and Zhang, 2013; Mohan et al., 2014). Some other inherent activities of photocatalyst include the transport of $e- h^+$ pairs, and efficient separation of photo-induced charge carriers (Niu et al., 2015b). (Luo and Maggard, 2006) have reported that $SrTiO_3$-coated with BFO nanoparticles can decompose water into H_2 and O_2 under visible light irradiation, whereas pure $SrTiO_3$ responds only to the UV irradiation. In addition, BFO nanowires decorated with Au nanoparticles can be used as highly efficient photocatalysts for water splitting (Li et al., 2013).

Investigation of BFO nanoparticle by doping with metals, non-metals and metalloids on the magnetic, electronic and the visible light-driven photoactivity of the material have been previously reported (Singh and Ishiwara, 2006; Hu et al., 2017; Jia et al., 2018; Haruna et al., 2019). BFO nanoparticle doped with some alkaline elements show improved magnetic properties and increased stability of the material (Bhushan et al., 2009). BFO nanoparticles have been synthesized by various methods and are used in the degradation and mineralization of dye pollutants. The effects of different pollutants on water and soil contamination were investigated using various methods by most researchers in modern technology to efficiently develop remediation processes (Ye et al., 2017a, 2017b). Also, the BFO and other related materials have been shown to be capable of utilizing visible light for photodegradation of molecules to harmless products. Several other visible light enhanced nanomaterials also find suitable applications in adsorption and photocatalytic process for the removal of pollutants such as tetracycline hydrochloride and bisphenol A (Ye et al., 2019; Wang et al., 2011a; Jing et al., 2013). In this review, an overview of some wet routes of synthesis of BFO nanoparticles have been briefly highlighted. Some recent progress on the effect of doping the material and the strategies to improve visible light response of the photocatalyst. The phenomenon of degradation process, mechanism of dye conversion and also a summary of future prospect for the development of the material all have been elaborated.

2. Synthesis of BFO nanoparticles

Various chemical methods have been used in the preparation of BFO and related nanopowders with characteristics of well crystalline, nano-size and absence of secondary phases, which are believed to be favorable for photocatalytic applications (Xian et al., 2011). These methods such as sol-gel, co-precipitation, hydrothermal, combustion, forced hydrolysis and microemulsion have been reported in an attempt to obtained powders with definite morphology, phase purity of the crystal, size and crystallinity of the material (Shami and Awan, 2011; Azam et al., 2011; Kuang et al., 2015; Kim, 2016; Haruna et al., 2019).

2.1. The sol-gel method

Sol-gel synthesis of nanoparticles is not new, the simplicity of the process for making functional oxides has been of keen interest to most researchers. This is because the method is handy and versatile, yield pure powders and can be used to fabricate materials that has very good surface area, size and morphology control (Pandey and Misha, 2011). The method is cost effective involving the reaction of metal nitrates in their stoichiometric proportions following the addition of suitable chelating and complexing agents. A homogeneous solution is usually formed and is set at a temperature between 80 – 90 °C under continuous heating and stirring until a sol is form. The sol is then dried to give gel and the gel is pre-calcined to give pure nanopowders. This technique has been used widely for the preparation of pure BFO and BFO related materials (Kuang et al., 2015; Abdulkadir et al., 2016; Haruna et al., 2018, 2019, 2020).

2.2. Co-precipitation method

The co-precipitation method is also simple for the preparation of perovskite-like compounds giving high yield. It gives particles of large grain size with poor homogeneity. Here, metal nitrates are precipitated by the action of soluble bases (NH_4OH) followed by subsequent washing and drying to yield powder nanoparticles. The as-prepared powder is annealed at various annealing temperatures to study a variety of a number of properties. The growth of the crystals, size and morphology of the crystallite can be controlled by adding surfactants like the polyvinyl acetate, triton x-100, sodium dodecyl sulfate, and cetyl trimethylammonium bromide (Mardani, 2017). The overall pH of the reacting process determines the products (Li et al., 1998).

2.3. Hydrothermal/solvothermal method

In this method of BFO and BFO related nanoparticle synthesis, the powders obtained are pure, regular in shape and highly dispersed with high crystallinity. The disadvantage of using this method is that raw materials for the synthesis must be for soluble salts, waste a lot of energy and is peculiar to Fe-based layered double hydroxide (Qu et al., 2016). It

is extremely important to note that from the photocatalytic point of view, nanomaterials obtained by this method have smaller sizes (20–80 nm), fewer defects, larger surface areas, and has special micro-/-nano-structures (Grabowska, 2016). It requires heating at temperature above 190 °C in a Parr bomb reactor under high pressure where the additives are dissolved in water or in organic solvent (Solvothermal). This method like the sol-gel process may also be accompanied by the addition of templating agents for structure directing, size control and crystal growth (Feng and Xu, 2000).

2.4. Mechanochemical method

This method requires high amount of energy as it commonly involve the ceramic fabrication during the milling procedure. It is a solvent free process, requiring lower temperature and shorter reaction time and the particles obtained by this process are regular hexagonal which together form the advantages of mechanochemistry over the hydrothermal method (Qu et al., 2016). Energy consumption and particles agglomeration are the disadvantages of this method. Metal oxides in their stoichiometric amounts are milled over some time to produce the fine powders. This is a typical of solid-state reaction and is very slow, and the reaction is activated due to mechanical process rather than application of temperature. This is because the long milling period is necessary to increase the reacting surfaces of the ions thereby creating more efficient interaction between the ions to form particles at room temperature (Stojanovic, 2003). Again, nanoparticles prepared by this method have the advantage of reduced calcination temperature.

2.5. Combustion

Combustion method is a self-sustaining exothermic reaction that occurs between metal salts and organic fuels to bring about the production of functional nanoparticles (Civera et al., 2003). This method produce nanomaterials with large particle sizes due to the high combustion temperature attained during the synthesis process (Kumar et al., 2009). The metal nitrates are made to dissolve in distilled water first, and to the solution of the metal nitrates, appropriate amount of sucrose is added with continuous stirring and placed on a hot plate until the dissolution process is complete. The mixture is further heated to obtain a dark viscous resins that leads to auto-ignition of the dried resin on continuous heating accompanying the evolution of gases (Farhadi and Zaidi, 2009). The ashes obtained from the combustion process is analyzed for perovskite-type BFO nanophase. Moreover, the size and shape of BFO materials greatly influence photocatalytic process and are generally controlled by adding templating agents (Lam et al., 2017).

3. Progress in the effect of doping of BFO nanoparticle

Various steps and strategies have been taken to modify the structure and increase the efficiency of BFO nanoparticles among which is the introduction of elements as dopants. The effect of doping nanocrystals of bismuth ferrites and orthoferrites is to improve the photocatalytic properties of the bulk materials. This has opened up newer opportunities in the area of photocatalysis. Generally, studies of the photocatalytic activity of these materials strongly depend on the particle size, morphology, crystallinity and surface chemistry (Tong et al., 2010). The photocatalytic properties of BFO and BFO related materials are size-dependent. Strong absorption of the catalyst in the visible region is achieved through particles with small sizes which give better surface area hence more active sites. Also, particles with high crystallinity are better achieved through prolonged heating and increased reaction time (Tong et al., 2010). The effect of crystallite size on the photocatalytic properties of BFO nanoparticles for the degradation of methyl orange (MO) with improved photoactivity have been reported (Gao et al., 2007). The results show more than 90 % of MO to be decolourized after 8 h of UV irradiation with reduced bandgap of 2.18 eV compared to the 2.5 eV value for BFO films (Takahashi and Tonouchi, 2007). Some researchers have worked on the photoelectrochemical process (PEC) of ferrites under visible light to investigate the photocatalytic hydrogen generation from water splitting although the mechanism is still not fully understood (Dillert et al., 2015; Gao et al., 2015; Banerjee et al., 2009; Mohapatra et al., 2009).

Almost all the rare earth metals; Y, La, Gd, Nd, Dy, Sm, have been introduced as dopants into the crystalline structure of BFO nanostructures to investigate the magnetic, optical, photocatalytic and electronic properties (Guo et al., 2010; Wu et al., 2013; Kaur et al., 2015; Sakar et al., 2015; Wei et al., 2016; Hu et al., 2017). Hu et al. reported the photocatalytic property of Sm doped BFO nanoparticle for the degradation of MO under visible light which showed reduce energy bandgap of 2.06 eV. Also, the visible light photodegradation of MB dye by BFO doped with Ba, Na and K metal ions in the presence of H_2O_2 was studied (Haruna et al., 2019). The smaller bandgap of the BFO-doped nanoparticles indicates a possibility of utilizing more visible light for photocatalysis. Also (Jaffari et al., 2019a), reported the hydrothermal synthesis of Pb-BFO catalyst for the degradation of malachite green dye and phenol from wastewater. The results show improved photoactivity of Pb doped to (95.7 %) compared to the pure BFO material (72.3 %) and TiO_2 (78.6 %). The enhanced photoactivity could be credited to the appropriate Pd contents that enhanced the e− trapping capacity, which was helpful in the generation and transmission of the generated e− h^+ pairs (Yilleng et al., 2018; Jaffari et al., 2019b).

The effect of doping BFO material, however, reduce the energy bandgap of the nanomaterials creating multiple energy trap states in between the valence band (VB) and conduction band (CB). When photon energy (*hv*) is absorbed equal to or higher than the bandgap energy, electrons (e−) are excited from the VB to the CB thereby creating holes (h^+) in the VB. These e− and h^+ created then initiate degradation process of the organic pollutants. The e− from the CB reacts with dissolved oxygen to generate highly reactive superoxide radicals ($O_2^{\bullet-}$) and H_2O_2 to oxidize the organic compounds (reduction process) (Lam et al., 2017). In a different reaction process, however, the holes generated can oxidize the organic pollutant by reacting with molecules of H_2O or OH on the surface of a photocatalyst to produce a highly reactive species such as hydroxyl radicals (oxidation process). The e− h^+ pairs generated under visible light, greatly enhanced the degradation efficiency of the catalyst.

The energy bandgap of BFO and BFO-doped semiconductor materials are shown in Figure 2 under visible light. The bandgap of undoped BFO can be seen to be wide due to e− h^+ recombination, but the effect of doping on BFO show reduced bandgap energy due to the decrease in recombination process. There is also the generation of multiple energy trap states between the VB and CB. Hence, the increase in the photocatalytic activity of the doped material which may be attributed to the efficient carrier charge separation produced by photo-excitation.

The photocatalytic activity, magnetic properties and other photophysical properties of the semiconducting BFO and other related materials are somewhat affected by the composition of the materials, method

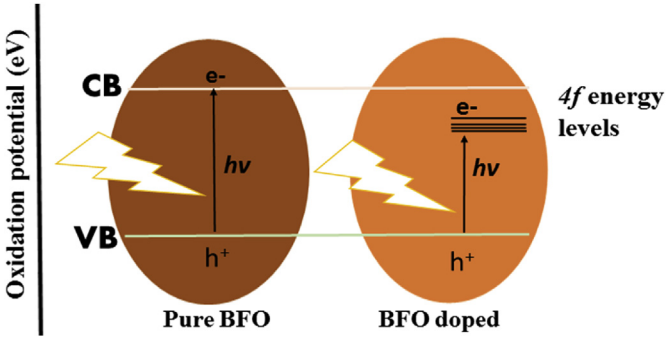

Figure 2. Schematic diagram on the effect of metal ion doping on the energy band gap of BFO nanoparticles.

of synthesis, their particle shapes and also size. Although the large particle size of nanomaterials could lead to a decrease in activity as a result of reducing the surface area of the catalyst, particle with smaller sizes tends to give better photoactivity due to the high number of active sites. A study shows the particle size in the range of 20–80 nm to give an added advantage for catalytic surfaces (Giannakas et al., 2006). (Ponraj et al., 2017) in their reviewed article on visible light active photocatalyst for degradation of different textile dyes, discussed the surface phenomenon of photocatalyst, particle size, and surface area and how they influence photocatalytic activity in great detail.

Doping of BFO nanoparticle especially with RE elements shows significant improvement on the photocatalytic properties of the material, this made possible the photogeneration of $e- h^+$ pairs due to the special 4f electron configurations of the elements (Mohan et al., 2014; Pei and Zhang, 2013; Wu et al., 2012). Co-doping of BFO with Sr, Ba, Ca, Na, K, have also been used to improve the photoactivity and visible light response of the material compared to the bulk BFO material. Table 1 shows the effect of crystallite size as estimated from the Debye-Scherrer relation in Eq. (1) for the doped and undoped BFO particles and how it affects the energy bandgap of the materials. The size of crystal significantly effects the photocatalytic activity due to easy transfer of charges to the surface of photocatalyst and the increased surface caused to provide more surface for incoming photo-generated charge carriers that absorbed more of the lights coming in (Irfan et al., 2019).

$$L = K\lambda/\beta\cos\theta \quad (1)$$

where L is the average crystallite size of the material, θ is the Bragg angle, K is the Scherrer constant, λ is the wavelength of radiation, and β is the full width at half maximum.

In another development, a study showed BFO doped with Dy enhance the photoactivity of MB degradation to 92 % under visible light irradiation (Sakar et al., 2015). The different methods of synthesis and the effect of doping into the structure of BFO and BFO related nanomaterials also influences the photocatalytic activity of the material as shown in Table 2 for comparison. BFO nanoparticles (average size of 29 nm) synthesized via the citric acid route by solvothermal process effectively degrade MB pollutants to 86 % having an energy value of 2.1 eV (Huo et al., 2010). The sol-gel synthesis of Ba doped BFO nanoparticle with a particle size of 23 nm showed very good photoactivity and reduced bandgap of 1.79 eV (Soltani and Lee, 2016; El-Desoky et al., 2016). A detailed study of the Na-doped BFO nanoparticle, its dielectric and multiferroic properties were previously reported (Zhang et al., 2014). The photocatalytic and magnetic properties, as well as the effect of the crystalline structure of Sr^{2+} doped BFO, was reported afte 2 h of visible light photo-response (Wang et al., 2012).

4. Phenomena of photodegradation studies

Some parameters such as the initial dye concentration, catalyst dosage, pH of the solution and the light source, affects the removal efficiency of BFO and BFO-doped photocatalyst. The energy bandgap of these nanomaterials can be calculated according to the well-known Tauc's Eq. (2) (Chang et al., 1995).

$$\alpha h\nu = C(h\nu - Eg)^{n/2} \quad (2)$$

where *Eg* is energy bandgap, α is the absorption coefficient, $h\nu$ is energy absorb, and C is a constant.

The % degradation efficiency for the dye removal during photocatalytic process is calculated using Eq. (3). Where C_0 and C_t are the initial and final concentrations of the dye before and after degradation process respectively.

$$\frac{C_o - C_t}{C_o} \times 100 \quad (3)$$

The photocatalytic properties of BFO and other related materials were previously researched for various pollutants degradation under visible light. Effect of dopants concentration, other conditions such as the effect of light source and initial dye concentration may influence the efficiency of the photocatalyst. Table 3 show the percentage of degradation of BFO and doped BFO materials on dyes with the effect of change in time, concentration and the source of light. For instance, the photocatalytic properties of BFO particles improved dramatically in the presence of La^{3+} ions for the degradation of Phenol red (Kaur et al., 2015). The degradation rate of MB dye from wastewater significantly improved on the addition of hydrogen peroxide promoted by the reduction of the dye to produce more reactive hydroxyl radicals in the photodegradation process. It is important therefore, to understand the mechanistic pathway for degradation of dyes in the photocatalytic studies of materials. Figure 3 shows the proposed mechanism for the photocatalytic degradation of a dye under visible light irradiation over the BFO-doped photocatalyst surface. The photocatalytic properties of BFO doped materials becomes more effective with a high charge separation of $e- h^+$. For a material that forms a kind of hetero-junction with BFO, it is generally believed to be effective in improving the photoactivity due to reduced recombination rate of the photogenerated electrons and holes (Mukherjee et al., 2012; Ge et al., 2011; Su et al., 2011; Wei et al., 2011). The visible light irradiation upon striking on the catalyst surface will initiate the photocatalytic reaction by absorbing light ($h\nu$) energy greater than or equal to its energy bandgap leading to the generation of $e- h^+$ pairs (detailed explanations in section 3) as seen in Eq. (4). Eqs. (5), (6), and (7) shows

Table 1. Effect of concentration and crystallite size on undoped BFO and rare-earth doped nanoparticles.

Research	BFO-doped	Conc of dopants	Space group	Lattice parameters			Crystallite size (nm)	Energy (eV)
				a (Å)	b (Å)	c (Å)		
Nadeem et al. (2018)	Ni	0.01	*R3c*	5.586	5.586	13.883	37	2.28
		0.05		5.644	5.644	14.013	14	2.29
Wang et al. (2011b)	BFO		*R3c*	5.576	5.576	13.867	20–35	2.55
Soltani and Entezari (2014)	BFO		*R3c*	5.576	5.576	13.867	20–35	2.20
	Impure			5.589	5.589	13.894	32.86	2.20
Majid et al. (2015)	BFO		*R3c*	5.528	5.528	13.721	28	-
Hu et al. (2017)	BFO		*R3c*	5.578	5.578	13.868	20–30	2.17
	Sm	0.01		5.577	5.577	13.862	17.2	2.15
	Sm	0.10		5.571	5.571	13.805	20–30	2.06
Zhang et al. (2016)	Gd	0.03	*R3c*	5.579	5.579	13.857	27.81	2.16
	Gd	0.05		5.571	5.571	13.830	27.71	2.10
Vanga et al. (2015)	BFO		*R3c*	5.578	5.578	13.847	30	2.02
	La	0.05		5.586	5.586	13.771	19	2.06
Wei et al. (2016)	Y	0.10	*R3c*	5.565	5.565	13.738	20–30	2.29

Table 2. Effect of synthesis method and crystallite size on the energy band gap of co-doped BFO.

Study	BFO-doped	Method of synthesis	Conc of dopants	Space group	Lattice parameters		Crystallite size (nm)	Energy (eV)
					a = b (Å)	c (Å)		
Wang et al. (2012)	Sr	Combustion	0.20	*P4/mmm*	3.954	3.954	22	2.26
El-Desoky et al. (2016) Soltani and Lee (2016)	Ba	Sol-gel	0.20	*R3c*	5.621	13.713	23	1.79
Haruna et al. (2019)	Na	Sol-gel	0.10	*R3c*	5.571	13.552	31	2.17
	K		0.10		5.578	13.542	28	2.15

Table 3. Percentage degradation efficiencies of undoped and doped BFO on dyes with effect of some parameters like the time, concentration and the source of light.

Research	BFO-doped	Dosage of catalyst (g)	Organic dye	Initial conc of dye (mg/L)	Light source	Time (min)	% Degradation
Vanga et al. (2016)	Gd, Sm	0.05	Methylene Blue	3.20	150 W He lamp	40	95
Mohan et al. (2014) Guo et al. (2010)	Gd		Methylene Blue	1.00	Sunlight	240	94
			Rhodamine B	5.00	500 W Xe lamp	120	94
Chen et al. (2015)	Nd	0.16	Rhodamine B	6.00	300 W Xe lamp	120	59
Mukherjee et al. (2012)	Y	0.01	Rhodamine B	50.00	40 W lamp	60	8
Kaur et al. (2015)	La	0.10	Phenol red	10.00	150 W Xe lamp	120	90
Sakar et al. (2015)	Dy	0.05	Methylene Blue	1.00	Sunlight	240	92
Li et al. (2009)	TiO_2	1:1	Congo red	-	500 W Xe lamp	120	70
Niu et al. (2015b)	Pt	0.25	Methyl orange	5.00	300 W Xe lamp	210	70
Di et al. (2014); Lu et al. (2015)	Ag	0.10	Rhodamine B	5.00	200 W Xe lamp	180	79
		0.05	Methyl orange	20.00	450 W Xe lamp	90	100
Wang et al. (2016)	Pb, Sm	0.30	Phenol	5.00	300 W Xe lamp	120	87
Jaffari et al. (2019a)	Pb	0.02	Malachite green	10.00	105 W vis lamp	240	96
Zhang et al. (2015)	Au	0.20	Congo red	20.00	500 W Xe lamp	120	94
Jia et al. (2018)	N	0.35	Bisphenol A	30.00	300W I/W lamp	120	94
Li et al. (2017)	N	0.02	Congo red	10.00	300 W Xe lamp	180	92

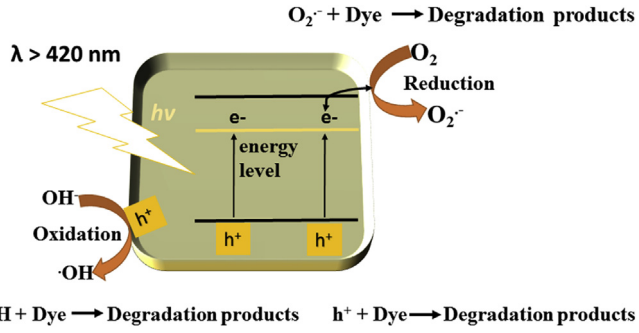

Figure 3. Schematic diagram of the mechanism of photocatalytic degradation of dye on doped BFO photocatalyst.

how the photogenerated electrons react with the surface adsorbed oxygen to form the superoxide radicals. The holes then reacts with water molecules to give hydroxyl radicals in Eq. (6). There is a simultaneous migration of holes onto the surface of the catalyst to react with water and form hydroxyl radicals which are very effective for the degradation of the dye, this is shown in Eq. (7). The superoxide radical generated then partake in the degradation process of the dye and usually, CO_2, H_2O, and other products are given off (mineralization). Eqs. (8) and (9) show direct oxidization of the dye by the catalyst based on the trapping experiments, the hydroxyl radical showed influence on the degradation pattern, the $O_2^{\bullet -}$ and h^+ generated were the predominant reactive species for the photodegradation studies of this material (Hu et al., 2017).

$$BFO - doped + hv \rightarrow e^- + h^+ \quad (4)$$

$$e^- + O_2 \longrightarrow O_2^- + H_2O_2 \quad (5)$$

$$h^+ + H_2O \longrightarrow OH \quad (6)$$

$$O_2^- + Dye \longrightarrow degradation\ products \quad (7)$$

$$\cdot OH + Dye \longrightarrow degradation\ products \quad (8)$$

$$h^+ + Dye \longrightarrow degradation\ products \quad (9)$$

The hydroxyl radicals, to a large extent, play important role in the photocatalytic oxidation process, and in photodegradation of dyes. Therefore, the effect of the addition of hydrogen peroxide will yield more hydroxyl radicals in the process hence a better photocatalytic result. Table 4 shows the effect of pH on the degradation pattern of some model dye pollutants.

5. A summary and outlook of future prospects of BFO nanoparticles

Doping of BFO nanomaterials with noble metals has been greatly utilized in increasing its efficiency as photocatalyst. The effect of synthesis method and change in size of the material has in various ways reduce the bandgap of the material towards the decolourization of dyes under visible light irradiation of the electromagnetic spectrum for photodegradation studies. Its nano-sized structure, multiferroic property at room temperature and crystal structure also makes BFO nanoparticles an efficient photocatalyst for degradation of pollutants. The doping effects of BFO and other related materials have shown improved photoactivity under visible light response very greatly. To date, a proper understanding of the mechanisms of the degradation process has been proposed by most researchers. A doped BFO material tends to offer a better charge separation phenomenon which influences the efficiency of the photocatalyst. The material because of its excellent chemical stability have been shown to be capable of treatment of wastewater and other industrial effluents

Table 4. Effect of pH on the percentage degradation rate of undoped and doped BFO on pollutants.

Research	BFO-doped	Organic dye	Initial conc of dye (mg/L)	pH	Time (min)	% Degradation
Vanga et al. (2015)	La	Methylene blue	3.20	2	50	96
Mohan et al. (2014)	Gd	Methylene blue	1.00	7	240	70
Ramadan et al. (2013)	Ca	Methylene blue	0.100	7	120	100
Soltani and Entezari (2013)		Methylene blue	15.00	2.5	120	70
Haruna et al. (2019)	Na	Methylene blue	10.00	3	100	60
				11	90	84
	K			3	100	56
				11	90	85
Yang et al. (2018)	Sr	Methylene blue	10.00	-	150	85

where they can also be successfully recovered. In some studies, the recyclability of the photocatalyst was tested to almost five cycles. Further research should be conducted on the computational studies of the material to understand the responsive mechanisms of the material towards dye degradation. Significant effort should be made also in future to commercialize BFO-doped particles for practical use in industries for wastewater treatment. The photoactivity of BFO-doped and BFO related nanomaterials should remain area of interest in the photodegradation of other pollutants, in particular; antibiotics, pesticides and other organic pollutants until exciting results are obtained.

Declarations

Author contribution statement

All authors listed have significantly contributed to the development and the writing of this article.

Funding statement

This research did not receive any specific grant from funding agencies in the public, commercial, or not-for-profit sectors.

Competing interest statement

The authors declare no conflict of interest.

Additional information

No additional information is available for this paper.

References

Abdulkadir, I., Jonnalagadda, S.B., Martincigh, B.S., 2016. Synthesis and effect of annealing temperature on the structural, magnetic and photocatalytic properties of $(La_{0.5}Bi_{0.2}Ba_{0.2}Mn_{0.1})FeO_{(3-d)}$. Mater. Chem. Phys. 178, 196–203.

Asahi, R., Morikawa, T., Ohwaki, T., Aoki, K., Taga, Y., 2001. Visible-light photocatalysis in nitrogen-doped titanium oxides. Science 293 (5528), 269–271.

Azam, A., Jawad, A., Ahmed, A.S., Chaman, M., Naqvi, A.H., 2011. Structural, optical and transport properties of Al3+ doped BiFeO3 nanopowder synthesized by solution combustion method. J. Alloy. Comp. 509 (6), 2909–2913.

Banerjee, S., Mohapatra, S.K., Misra, M., 2009. Synthesis of TaON nanotube arrays by sonoelectrochemical anodization followed by nitridation: a novel catalyst for photoelectrochemical hydrogen generation from water. Chem. Commun. (46), 7137.

Bhushan, B., Basumallick, A., Bandopadhyay, S.K., Vasanthacharya, N.Y., Das, D., 2009. Effect of alkaline earth metal doping on thermal, optical, magnetic and dielectric properties of BiFeO3 nanoparticles. J. Phys. D Appl. Phys. 42, 065004.

Carp, O., Huisman, C.L., Reller, A., 2004. Photoinduced reactivity of titanium dioxide. Prog. Solid State Chem. 32 (1-2), 33–177.

Chang, D.A., Lin, P., Tseng, T.Y., 1995. Optical properties of $ZrTiO_4$ films grown by radio-frequency magnetron sputtering. J. Appl. Phys. 77, 4445–4451.

Chen, X., Mao, S.S., 2007. Titanium dioxide nanomaterials: synthesis, properties, modifications, and applications. Chem. Rev. 107 (7), 2891–2959.

Chen, Z., Wu, Y., Wang, X., Jin, W., Zhu, C., 2015. Ferromagnetism and enhanced photocatalytic activity in Nd doped $BiFeO_3$ nanopowders. J. Mater. Sci. Mater. Electron. 26, 9929–9940.

Cheng, Z., Lin, J., 2010. Layered organic-inorganic hybrid perovskite: structure, optical properties, film preparation, patterning and templating engineering. Crystal Eng. Commun. 12, 2646–2662.

Civera, A., Pavese, M., Saracco, G., Specchia, V., 2003. Combustion synthesis of perovskite-type catalysts for natural gas combustion. Catal. Today 83 (1–4), 199–211.

Di, L.J., Yang, H., Hu, G., Xian, T., Ma, J.Y., Jiang, J.L., Li, R.S., Wei, Z.Q., 2014. Enhanced photocatalytic activity of BiFeO3 particles by surface decoration with Ag nanoparticles. J. Mater. Sci. Mater. Electron. 25, 2463–2469.

Dillert, R., Taffa, D.H., Wark, M., Bredow, T., Bahnemann, D.W., 2015. Research Update: photoelectrochemical water splitting and photocatalytic hydrogen production using ferrites (MFe_2O_4) under visible light irradiation. Apl. Mater. 3 (10), 104001.

El-Desoky, M.M., Ayoua, M.S., Mostafa, M.M., Ahmed, M.A., 2016. Multiferroic properties of nanostructured barium doped bismuth ferrite. J. Magn. Magn. Mater. 404, 68–73.

Farhadi, S., Zaidi, M., 2009. Bismuth ferrite (BiFeO3) nanopowder prepared by sucrose-assisted combustion method: a novel and reusable heterogeneous catalyst for acetylation of amines, alcohols and phenols under solvent-free conditions. J. Mol. Catal. A Chem. 299, 18–25.

Feng, S., Xu, R., 2000. New materials in hydrothermal synthesis. Acc. Chem. Res. 34, 239–247.

Gao, B.F., Chen, X., Yin, K., Dong, S., Ren, Z., Yuan, F., Zou, Z., 2007. Visible-Light Photocatalytic Properties of Weak Magnetic $BiFeO_3$ Nanoparticles, pp. 2889–2892.

Gao, T., Chen, Z., Huang, Q., Niu, F., Huang, X., Qin, L., Huang, Y., 2015. A review: preparation of bismuth ferrite nanoparticles and its applications in visible-light induced photocatalyses. Rev. Adv. Mater. Sci. 40 (2), 97–109.

Ge, M., Li, Y., Liu, L., Zhou, Z., Chen, W., 2011. Bi_2O_3–Bi_2WO_6 composite microspheres: hydrothermal synthesis and photocatalytic performances. J. Phys. Chem. C 115 (13), 5220–5225.

Giannakas, A.E., Leontiou, A.A., Ladavos, A.K., Pomonis, P.J., 2006. Characterization and catalytic investigation of NO + CO reaction on perovskites of the general formula $La_xM_{1-x}FeO_3$ (M = Sr and/or Ce) prepared via a reverse micelles microemulsion route. Appl. Catal. A Gen. 309, 254–262.

Grabowska, E., 2016. Selected perovskite oxides: characterisation, preparation and photocatalytic properties – a review. Appl. Catal. B Environ. 186, 97–126.

Green, M.A., Ho-Baillie, A., Snaith, H.J., 2014. The emergence of perovskite solar cells. Nat. Photonics 8, 506–514.

Guo, R., Fang, L., Dong, W., Zheng, F., Shen, M., 2010. Enhanced photocatalytic activity and ferromagnetism in Gd doped $BiFeO_3$ Nanoparticles. J. Phys. Chem. C 114, 21390–21396.

Haruna, A., Abdulkadir, I., Idris, S.O., 2018. Visible light induced photodegradation of methylene blue in sodium doped bismuth barium ferrite nanoparticle synthesized by sol-gel method. Avicenna J. Environ. Health Eng. 5 (2), 120–126.

Haruna, A., Abdulkadir, I., Idris, S.O., 2019. Synthesis, characterization and photocatalytic properties of $Bi_{0.85-X}M_XBa_{0.15}FeO_3$ (M = Na and K, X=0, 0.1) perovskite-like nanoparticles using the sol-gel method. J. King Saud Univ. Sci.

Haruna, A., Abdulkadir, I., Idris, S.O., 2020. Effect of annealing temperature on the synthesis and photocatalytic properties of $Bi_{0.65}K_{0.2}Ba_{0.15}FeO_3$ perovskite-like nanoparticle synthesized by sol-gel method. Beni-Suef Univ. J. Basic Appl. Sci. (Article in press).

He, J., Guo, R., Fang, L., Dong, W., Zheng, F., Shen, M., 2013. Characterization and visible light photocatalytic mechanism of size-controlled. Mater. Res. Bull. 48 (9), 3017–3024.

Hu, Z., Chen, D., Wang, S., Zhang, N., Qin, L., Huang, Y., 2017. Facile synthesis of Sm-doped $BiFeO_3$ nanoparticles for enhanced visible light photocatalytic performance. Mater. Sci. Eng. B 220, 1–12.

Huo, Y., Jin, Y., Zhang, Y., 2010. Citric acid assisted solvothermal synthesis of $BiFeO_3$ microspheres with high visible-light photocatalytic activity. J. Mol. Catal. A Chem. 331 (1–2), 15–20.

Irfan, S., Zhuanghao, Z., Li, F., Chen, Y., Liang, G., Luo, J., Ping, F., 2019. Critical review: bismuth ferrite as an emerging visible light active nanostructured photocatalyst. J. Mater. Res. Technol.

Jaffari, Z.H., Lam, S.-M., Sin, J.-C., Zeng, H., Rahman, M.A., 2019a. Magnetically recoverable Pd-loaded $BiFeO_3$ microcomposite with enhanced visible light photocatalytic performance for pollutant, bacterial and fungal elimination. Separ. Purif. Technol. 116195.

Jaffari, Z.H., Lam, S., Sin, J., Zeng, H., 2019b. Boosting visible light photocatalytic and antibacterial performance by decoration of silver on magnetic spindle-like bismuth ferrite. Mater. Sci. Semicond. Process. 101, 103–115.

Jia, Y., Wu, C., Kim, D.-H., Lee, B.W., Rhee, S.J., Park, Y.C., et al., 2018. Nitrogen doped $BiFeO_3$ with enhanced magnetic properties and photo-Fenton catalytic activity for degradation of bisphenol A under visible light. Chem. Eng. J. 337, 709–721.

Jiang, J.Z., Zou, J., Naveed, M.A., Yan, J.C., Huang, L., Zhang, Y.X., Chen, J., 2011. Synthesis and characterization of wafer-like BiFeO3 with efficient catalytic activity. Solid State Sci. 13 (9), 1779–1785.

Jing, L., Zhou, W., Tian, G., Fu, H., 2013. Surface tuning for oxide-based nanomaterials as efficient photocatalysts. Chem. Soc. Rev. 42, 9509–9549.

Kanhere, P., Chen, Z., 2014. A review on visible light active perovskite-based photocatalysts. Molecules 19 (12), 19995–20022.

Kaur, M., Yadav, K.L., Uniyal, P., 2015. Investigations on multiferroic, optical and photocatalytic properties of lanthanum doped bismuth ferrite nanoparticles. Adv.Mater. Lett . 6, 895–901.

Kim, J.Y., 2016. Low-temperature hydrothermal synthesis of pure $BiFeO_3$ nanopowders using triethanolamine and their applications as visible-light photocatalysts, 3755 (24913), 3753–3755.

Kuang, D., Tang, P., Ding, X., Yang, S., Zhang, Y., 2015. Effects of Y doping on multiferroic properties of sol-gel deposited $BiFeO_3$ thin films. J. Mater. Sci. Mater. Electron. 26, 3001–3007.

Kumar, M., Srikanth, S., Ravikumar, B., Alex, T.C., Das, S.K., 2009. Synthesis of pure and Sr-doped $LaGaO_3$, $LaFeO_3$ and $LaCoO_3$ and Sr,Mg-doped $LaGaO_3$ for ITSOFC application using different wet chemical routes. Mater. Chem. Phys. 113 (2-3), 803–815.

Lam, S., Sin, J., Mohamed, A.R., 2017. A newly emerging visible light-responsive $BiFeO_3$ perovskite for photocatalytic applications: a mini review. Mater. Res. Bull. 90, 15–30.

Li, Y., Liao, H., Qian, Y., 1998. Hydrothermal synthesis of ultrafine α-Fe_2O_3 and Fe_3O_4 powders. Mater. Res. Bull. 33, 841–844.

Li, S., Lin, Y.H., Zhang, B.P., Li, J.F., Nan, C.W., 2009. $BiFeO_3/TiO_2$ core-shell structured nanocomposites as visible-active photocatalysts and their optical response mechanism. J. Appl. Phys. 105 (5), 054310.

Li, S., Zhang, J., Kibria, M.G., Mi, Z., Chaker, M., Ma, D., Nechache, R., Rosei, F., 2013. Remarkably enhanced photocatalytic activity of laser ablated Au nanoparticle decorated $BiFeO_3$ nanowires under visible-light. Chem. Commun. 49 (52), 5856–5858.

Li, P., Li, L., Xu, M., Chen, Q., He, Y., 2017. Enhanced photocatalytic property of $BiFeO_3$/N-doped graphene composites and mechanism insight. Appl. Surf. Sci. 396, 879–887.

Liu, J.M., Gao, F., Chen, X., Yin, K., Dong, S., Ren, Z., Yuan, F., Yu, T., Zou, Z., 2007. Visible-light photocatalytic properties of weak magnetic $BiFeO_3$ nanoparticles. Adv. Mater. 19, 2889–2892.

Liu, F., Lai, S., Huang, P., Liu, Y., Xu, Y., Fang, Y., Zhou, W., 2012. Fabrication and photocatalytic activity of TiO2 derived nanotubes with Ag ions doping. J. Nanosci. Nanotechnol. 12 (11), 8391–8395.

Lu, H., Du, Z., Wang, J., Liu, Y., 2015. Enhanced photocatalytic performance of Ag-decorated $BiFeO_3$ in visible light region. J. Sol. Gel Sci. Technol. 76, 50–57.

Luo, J., Maggard, P.A., 2006. Hydrothermal synthesis and photocatalytic activities of $SrTiO_3$-coated Fe_2O_3 and $BiFeO_3$. Adv. Mater. 18 (4), 514–517.

Maeda, K., Domen, K., 2007. New non-oxide photocatalysts designed for overall water splitting under visible light. J. Phys. Chem. 111, 7851–7861.

Majid, F., Mirza, S.T., Riaz, S., Naseem, S., 2015. Sol-gel synthesis of $BiFeO_3$ nanoparticles. Mater. Today Proceedings 2 (10), 5293–5297.

Mardani, R., 2017. The synthesis of Ba^{2+}-doped multiferroic $BiFeO_3$ nanoparticles using co-precipitation method in the presence of various surfactants and the investigation of structural and magnetic features. Mod. Phys. Lett. B 31 (15), 1750169.

Mohan, S., Subramanian, B., Bhaumik, I., Gupta, P.K., Jaisankar, S.N., 2014. Nanostructured $Bi_{(1-x)}Gd_{(x)}FeO_3$ – a multiferroic photocatalyst on its sunlight driven photocatalytic activity. RSC Adv. 4, 16871–16878.

Mohapatra, S.K., John, S.E., Banerjee, S., Misra, M., 2009. Water photooxidation by smooth and ultrathin α-Fe2O3Nanotube Arrays. Chem. Mater. 21 (14), 3048–3055.

Moniruddin, M., Ilyassov, B., Zhao, X., Smith, E., Serikov, T., Ibrayev, N., Nuraje, N., 2018. Recent progress on perovskite materials in photovoltaic and water splitting applications. Mater. Today Energy 7, 246–259.

Mukherjee, A., Hossain, Sk.M., Pal, M., Basu, S., 2012. Effect of Y-doping on optical properties of multiferroics $BiFeO_3$ nanoparticles. Appl. Nanosci. 2, 305–310.

Nadeem, M., Khan, W., Khan, S., Shoeb, M., Husain, S., Mobin, M., 2018. Significant enhancement in photocatalytic performance of Ni doped BiFeO3 nanoparticles. Mater. Res. Express 5 (6), 065506.

Niu, F., Chen, D., Qin, L., Gao, T., Zhang, N., Wang, S., Chen, Z., Wang, J., Sun, X., Huang, Y., 2015a. Synthesis of Pt/$BiFeO_3$ heterostructured photocatalysts for highly efficientvisible-light Photocatalytic performances. J. Solar Energy Mater. Solar Cells 143, 386–396.

Niu, F., Gao, T., Zhang, N., Chen, Z., Huang, Q., Qin, L., Sun, X., Huang, Y., 2015b. Hydrothermal synthesis of $BiFeO_3$ nanoparticles for visible light photocatalytic applications. J. Nanosci. Nanotechnol. 15 (12), 9693–9698.

Pandey, S., Misha, S., 2011. Sol–gel derived organic–inorganic hybrid materials: synthesis, characterizations and applications. J. Sol. Gel Sci. Technol. 59, 73–94.

Park, N.-G., 2016. Crystal growth engineering for high efficiency perovskite solar cells. Crystal Eng. Commun. 18 (32), 5977–5985.

Pei, Y.L., Zhang, C.L., 2013. Effect of ion doping in different sites on the morphology and photocatalytic activity of $BiFeO_3$ microcrystals. J. Alloy. Comp. 570, 57–60.

Ponraj, C., Vinitha, G., Daniel, J., 2017. A review on the visible light active $BiFeO_3$ nanostructures as suitable photocatalyst in the degradation of different textile dyes. J. Environ. Nanotechnol. Monit. Manag. 7, 110–120.

Qu, J., Zhang, Q., Li, X., He, X., Song, S., 2016. Mechanochemical approaches to synthesize layered double hydroxides: a review. Appl. Clay Sci. 119, 185–192.

Rajeshwar, K., Osugi, M.E., Chanmanee, W., Chenthamarakshan, C.R., Zanoni, M.V.B., Kajitvichyanukul, P., Krishnan-Ayer, R., 2008. Heterogeneous photocatalytic treatment of organic dyes in air and aqueous media. J. Photochem. Photobiol. C 9, 171–192.

Ramadan, W., Shaikh, P.A., Ebrahim, Sh., Ramadan, A., Hannoyer, B., Jouen, S., Sauvage, X., Ogale, S., 2013. Highly efficient photocatalysis by $BiFeO_3$/α(γ)-Fe_2O_3 ferromagnetic nano p/n junctions formed by dopant-induced phase separation. J. Nanoparticle Res. 15, 1848.

Sakar, M., Balakumar, S., Saravananb, P., Bharathkumar, S., 2015. Compliments of confinements: substitution and dimension induced magnetic origin and band bending mediated photocatalytic enhancements in Bi $_{1-x}Dy_xFeO_3$ particulate and fibernanostructures. Nanoscale 7, 10667–10679.

Shami, M.Y., Awan, M.S., 2011. Phase pure synthesis of BiFeO3 nanopowders using diverse precursor via co-precipitation method. J. Alloy. Comp. 509 (41), 10139–10144.

Shi, J., Guo, A.L., 2013. ABO3 -based photocatalysts for water splitting. Prog. Nat. Sci. Mater. Int. Rev. 22 (6), 592–615.

Singh, S.K., Ishiwara, H., 2006. Doping effect of rare-earth ions on electrical properties ofBiFeO $_3$ thin films fabricated by chemical solution method. Jpn J. Appl. Phys. 45, 3194–3197.

Soltani, T., Entezari, M.H., 2013. Photolysis and photocatalysis of methylene blue by ferrite bismuth nanoparticles under sunlight irradiation. J. Mol. Catal. A Chem. 377 (3), 197–203.

Soltani, T., Entezari, M.H., 2014. Solar-Fenton catalytic degradation of phenolic compounds by impure bismuth ferrite nanoparticles synthesized via ultrasound. Chem. Eng. J. 251, 207–216.

Soltani, T., Lee, B.K., 2016. Novel and facile synthesis of Ba-doped $BiFeO_3$ nanoparticles and enhancement of their magnetic and photocatalytic activities for complete degradation of benzene in aqueous solution. J. Hazard Mater. 316. Elsevier B.V.

Stojanovic, B.D., 2003. Mechanochemical synthesis of ceramic powders with perovskite structure. J. Mater. Process. Technol. 143, 78–81.

Su, J., Guo, L., Bao, N., Grimes, C.A., 2011. Nanostructured WO_3/$BiVO_4$ heterojunction films for efficient photoelectrochemical water splitting. Nano Lett. 11 (5), 1928–1933.

Takahashi, K., Tonouchi, M., 2007. Influence of manganese doping in multiferroic bismuth ferrite thin films. J. Magn. Magn. Mater. 310, 1174–1176.

Tanaka, H., Misano, M., 2001. Advances in designing perovskite catalysts. Curr. Opin. Solid State Mater. Sci. 5, 381–387.

Tong, W., Li, L., Hu, W., Yan, T., Li, G., 2010. Systematic control of monoclinic $CdWO_4$ nanophase for optimum photocatalytic activity. J. Phys. Chem. C 114 (3), 1512–1519.

Vanga, P.R., Mangalaraja, R.V., Ashok, M., 2015. Structural, magnetic and photocatalytic properties of La and alkaline co-doped $BiFeO_3$ nanoparticles. Mater. Sci. Semicond. Process. 40, 796–802.

Vanga, P.R., Mangalaraja, R.V., Ashok, M., 2016. Effect of co-doping on the optical, magnetic and photocatalytic properties of the Gd modified $BiFeO_3$. J. Mater. Sci. Mater. Electron. 27 (6), 5699–5706.

Wang, N., Zhu, L., Lei, M., She, Y., Cao, M., Tang, H., 2011a. Ligand-induced drastic enhancement of catalytic activity of nano-$BiFeO_3$ for oxidative degradation of bisphenol A. ACS Catal. 1, 1193–1202.

Wang, X., Lin, Y., Zhang, Z.C., Bian, J.Y., 2011b. Photocatalytic activities of multiferroic bismuth ferrite nanoparticles prepared by glycol-based sol–gel process. J. Sol. Gel Sci. Technol. 60, 1–5.

Wang, B., Wang, S., Gong, L., Zhou, Z., 2012. Structural, magnetic and photocatalytic properties of Sr2-doped $BiFeO_3$ nanoparticles based on an ultrasonic irradiation assisted self-combustion method. Ceram. Int. 38 (8), 6643–6649.

Wang, S., Chen, D., Niu, F., Zhang, N., Qin, L., Huang, Y., 2016. Pd cocatalyst on Sm-doped $BiFeO_3$ nanoparticles: synergetic effect of a Pd cocatalyst and samarium doping on photocatalysis. RSC Adv. 6, 34574–34587.

Wei, X., Xie, T., Peng, L., Fu, W., Chen, J., Gao, Q., et al., 2011. Effect of heterojunction on the behavior of photogenerated charges in Fe_3O_4@Fe_2O_3 nanoparticle photocatalysts. J. Phys. Chem. C 115 (17), 8637–8642.

Wei, J., Liu, Y., Bai, X., Li, C., Liu, Y., Xu, Z., Gemeiner, P., Haumont, R., Infante, I.C., Dkhil, B., 2016. Crystal structure, leakage conduction mechanism evolution and enhanced multiferroic properties in Y-doped $BiFeO_3$ ceramics. Ceram. Int. 42, 13395–13403.

Wu, S.X., Fang, J.Z., Xu, X.X., Liu, Z., Zhu, X.M., Xu, W.C., 2012. Microemulsion synthesis, characterization of highly visible light responsive rare earth-doped Bi_2O_3. Photochem. Photobiol. 88, 1205–1210.

Wu, C., Wei, J., Kong, F., 2013. Effect of rare earth dopants on themorphologies and photocatalytic activities of BiFeO $_3$ microcrystallites. J. Mater. Sci. Mater. Electron. 24, 1530–1535.

Xian, T., Yang, H., Dai, J.F., Wei, Z.Q., Ma, J.Y., Feng, W.J., 2011. Photocatalytic properties of $BiFeO_3$ nanoparticles with different sizes. Mater. Lett. 65 (11), 1573–1575.

Yang, Y., Sun, Y., Jiang, Y., 2006. Structure and photocatalytic property of perovskite and perovskite-related compounds. Mater. Chem. Phys. 96 (2–3), 234–239.

Yang, R., Sun, H., Li, J., Li, Y., 2018. Structural, magnetic and photocatalytic properties of Sr^{2+} doped $BiFeO_3$ nanofibres fabricated by electrospinning. Ceram. Int. 44 (12), 14032–14035.

Ye, S., Zeng, G., Wu, H., Zhang, C., Dai, J., Liang, J., et al., 2017a. Critical Reviews in Biotechnology Biological technologies for the remediation of co- contaminated soil. Crit. Rev. Environ. Sci. Technol. 47, 1528–1553.

Ye, S., Zeng, G., Wu, H., Zhang, C., Liang, J., Dai, J., 2017b. Co-occurrence and interactions of pollutants , and their impacts on soil remediation — a review. Crit. Rev. Biotechnol. 37 (8), 1062–1076.

Ye, S., Yan, M., Tan, X., Liang, J., Zeng, G., Wu, H., et al., 2019. Facile assembled biochar-based nanocomposite with improved graphitization for efficient photocatalytic activity driven by visible light. Appl. Catal. B Environ. 250, 78–88.

Yilleng, M.T., Gimba, E.C., Ndukwe, G.I., Bugaje, I.M., Rooney, D.W., Manyar, H.G., 2018. Batch to continuous photocatalytic degradation of phenol using TiO_2 and Au-Pd nanoparticles supported on TiO_2. J. Environ. Chem. Eng. 6, 6382–6389.

Yu, X.L., Wang, Y., Hu, Y.M., Cao, C.B., Chan, Helen Lai-Wa, 2009. Gas sensing properties of perovskite BiFeO3 nanoparticles. J. Am. Ceram. Soc. 92, 3105–3107.

Zeches, R.J., Rossell, M.D., Zhang, J.X., Hatt, A.J., He, Q.E., Yang, C.H., Kumar, A., Wang, C.H., Melville, A., Ada, C., 2009. A strain-driven morphotropic phase boundary in BiFeO3. Science 326, 977–980.

Zhang, Q., Xu, H., Yan, W., 2012. Highly ordered TiO_2 nanotube Arrays: recent advances in fabrication and environmental applications—a review. Nanosci. Nanotechnol. Lett. 4 (5), 505–519 (15).

Zhang, H., Liu, W., Wu, P., Hai, X., Guo, M., Xi, X., et al., 2014. Novel behaviors of multiferroic properties in Na-Doped $BiFeO_3$ nanoparticles. Nanoscale 6 (18), 10831–10838.

Zhang, Y., Cai, Z., Ma, X., 2015a. Photocatalysis enhancement of Au/BFO nanoparticles using plasmon resonance of Au NPs. Phys. B Condens. Matter 479, 101–106.

Zhang, X., Wang, B., Wang, X., Xiao, X., Dai, Z., Wu, W., Zheng, J., Ren, F., Jiang, C., 2015b. Preparation of M@$BiFeO_3$ nanocomposites (M = Ag, Au) bowl arrays with enhanced visible light photocatalytic activity. J. Am. Ceram. Soc. 98 (7), 2255–2263.

Zhang, N., Chen, D., Niu, F., Wang, S., Qin, L.S., Huang, Y.X., 2016. Enhanced visible light photocatalytic activity of Gd-doped $BiFeO_3$ nanoparticles and mechanism insight. Sci. Rep. 6, 26467.

Zhao, D., Chen, C.C., Wang, Y.F., Ma, W.H., Zhao, J.C., Rajh, T., Zang, L., 2008. Enhanced photocatalytic degradation of dye pollutants under visible irradiation on Al(III)-Modified TiO2: structure, interaction, and interfacial electron transfer. Environ. Sci. Technol. 42, 308–314.